

Available Acceleration Set for the Study of Motion Capabilities for Cable-Driven Robots

Jonathan Eden^{a,*}, Darwin Lau^b, Ying Tan^a, Denny Oetomo^a

^aMelbourne School of Engineering, The University of Melbourne, Victoria, Australia

^bDepartment of Mechanical and Automation Engineering, The Chinese University of Hong Kong, Hong Kong

Abstract

The study of the ability of a cable driven robot (*CDR*) to generate motion between poses (*motion generation capability*) is important for many purposes such as motion planning and manipulator design. Existing analysis approaches that study CDR capability primarily do so by evaluating the mechanism's wrench generation abilities. Due to the nonlinear relationship between wrench and motion generation, these methods typically underestimate the true motion generation capability of a CDR and can result in conservative restrictions in operation. In this paper, two new metrics derived from the available acceleration set are proposed to better understand CDR motion generation capability. Using these metrics and the known properties of the static workspace, the maximum acceleration and speed capabilities of the CDR are quantified. This new information serves to better inform other technical aspects in the design, analysis and operation of CDRs, such as in workspace design and motion planning. To illustrate the application of the proposed metrics, two example robots are considered: a 2 link 2 DoF 4 cable CDR and a 6 DoF 7 cable CDR. The results show the insights into motion generation and how it provides new information to be used within motion planning and task scaling.

Keywords: Cable-driven robots, Motion generation analysis, Static workspace

1. Introduction

Cable driven robots (CDRs) are a class of mechanism where cable actuators are used in place of rigid links. The advantages of CDRs include: increased reconfigurability, higher payload to weight ratio and potentially larger workspaces. With these benefits, CDRs have been studied for a range of applications including high-speed manufacturing [1], environment sensing [2], rehabilitation [3] and the analysis of musculoskeletal systems [4].

A unique feature in the study of CDRs is that the actuating cables can only operate under tension (*positive cable force*). This results in actuation redundancy and constraints on the system dynamics, creating challenges in the control and analysis of these mechanisms [5, 6, 7]. As a result, the analysis of system kinematics alone is not sufficient to determine if the manipulator has the capability to generate motion from one pose to another (*motion generation capability*). Understanding of this capability is important in the design [6, 8], trajectory planning [5, 9, 10, 11] and construction of paths for CDRs. Typically, analyses of CDR capability consider the ability of the CDR to produce a set of desired wrenches [12, 13, 14]. This analysis has predominately been performed using two tools: workspace metrics and workspace conditions.

Workspace metrics quantify a manipulator's capability by studying the set of wrenches that the CDR can generate (*available wrench set*). Examples of metrics include dexterity [15, 16], tension factor [17] and capacity margin [14, 18]. Dexterity and tension factor describe the distribution of cable forces in

*Corresponding Author

Email addresses: jpeden@student.unimelb.edu.au (Jonathan Eden), darwinlau@mae.cuhk.edu.hk (Darwin Lau), yingt@unimelb.edu.au (Ying Tan), doetomo@unimelb.edu.au (Denny Oetomo)

producing arbitrary wrenches. The *capacity margin* represents the shortest signed distance between the set of wrenches to be generated (*desired wrench set*) and the available wrench set, providing a measure of the CDR's robustness in producing the desired wrench set. Existing CDR metrics primarily focus on desirable manipulation qualities for the design of CDRs and therefore perform the analysis on the wrench set. However, wrench capability does not necessarily reflect the ability of the mechanism to produce motion. For motion generation purposes, an accurate measure of capability can be determined by direct analysis of the available set of joint velocities and accelerations. In serial robots, metrics such as dynamic manipulability [19] have been used to analyse the capability of the robot to produce acceleration, however, this class of metric does not take into account the unilateral actuation characteristics of CDRs.

While workspace metrics describe the wrench generation quality of the manipulator, *workspace conditions* define whether a set of wrenches or motions can be produced at a particular pose. Using these conditions, workspace analysis allows the capabilities of the manipulator to be studied by identifying the set of poses for which a workspace condition is satisfied. A range of different workspace conditions have been studied to consider different types of CDR capabilities, including the *static workspace* [20, 5], *dynamic workspace* [21], *wrench-feasible workspace* [13, 22] and *wrench-closure workspace* [17, 23, 24].

The wrench-closure workspace (*WCW*) is a commonly studied type of workspace that is defined as the set of poses in which any wrench can be produced when assuming that all cable forces are positive and unbounded [23]. While the WCW has not been typically used to analyse motion generation, the ability to produce any wrench means that the CDR is capable of producing all joint velocities and accelerations. This means that any trajectory that lies within a connected region of the WCW can be executed [25]. However, since motion generation only requires that there exists a single trajectory to connect two points, the generation of wrenches in all directions is not necessary. The WCW is therefore a conservative representation of the set of poses for which motions can be generated between, limiting its usefulness in the study of motion generation capabilities. Furthermore, the WCW may not be practical for motion generation of physical CDRs as the actual bounds of cable forces are not considered.

The wrench-feasible workspace (*WFW*) considers the set of all poses for which the desired wrench set can be produced using given upper and lower bounds on the cable forces [12]. The use of the WFW can result in less conservative estimates of the set of all poses for which a motion can be generated, by considering only the subset of directions required. However, since both the WCW and WFW specify the desired set in the wrench space, the choice of an appropriate wrench set for the purpose of motion generation is not clear due to the effect of the nonlinear mapping between kinematic and kinetics.

The dynamic workspace (*DW*) considers the set of all poses for which a desired set of accelerations and velocities can be produced using given upper and lower bounds on the cable forces [21]. Although this workspace directly considers accelerations, velocities and bounds on the cable forces, it is difficult to prescribe a desired set of accelerations and velocities in advance for analysing motion generation capability. A special case of the dynamic workspace is the static workspace (*SW*), where the desired accelerations and velocities are set to be zero [26], representing the set of all poses for which the CDR can sustain gravity. The SW has been suggested to have potential application in motion generation through task scaling [5, 27]. However, since this workspace only guarantees that the manipulator can remain in static equilibrium, the application of the SW to the study of motion generation has been limited. As such, if the capability of the CDR within the SW could be quantified, then the use of SW would be much more advantageous in the study of motion generation since it typically represents a much larger set of poses than other workspaces.

In this paper, two new workspace metrics are proposed for the analysis of motion generation capability within the SW. These metrics are obtained through the direct analysis of the acceleration space, where the available acceleration set is introduced as the set of accelerations that can be produced by the CDR for a given range of cable force bounds. From this set, the *acceleration capability metric* is defined as the minimum signed distance between the available and desired acceleration sets. This proposed metric provides an intuitive measure of the CDRs additional capability to generate motion at poses within the dynamic and static workspaces. It is also shown that poses within the static workspace with positive acceleration capability measure hold the property of local positive controllability. Using positive controllability theory [28, 29, 30] and the acceleration capability measure, the *maximum controllable speed* metric is then proposed as an estimate of the maximum speed at which the positive controllability property is maintained for poses

within the SW. The insight into motion generation capability provided by these two new metrics is then shown through the consideration of two different case study CDRs, where the advantages of using the static workspace in combination with the capability measure for motion generation analysis are highlighted. These simulations are performed using CASPR: an open-source cable robotics analysis and simulation platform [31].

The primary motivation of this study is to increase the understanding of motion generation capability through the establishment of new metrics. Metrics derived in the acceleration space, represent direct metrics on the CDR's capability to alter its kinematics. These metrics can be made trajectory independent, such that they can provide new insight into a range applications including CDR design, task scaling and path planning. Most of the existing analysis of CDR capability has made use of wrench based techniques. These techniques can only be related to the system's kinematics through a nonlinear velocity dependent equation of motion, such that they are typically trajectory dependent and not proportional to acceleration capability. Metrics obtained through direct analysis of the acceleration space therefore offer additional insight, by more accurately quantifying the ability to produce motion which adds qualitative understanding of the CDR's true capability within the SW.

The remainder of the paper is organised as follows: Section 2 presents the background on wrench set analysis and the capacity margin. Section 3 introduces the available acceleration set and the acceleration capability measure. Using this measure, Section 4 presents sufficient conditions for the positive controllability of CDRs and then presents the maximum controllable speed metrics as an estimate of the maximum speed at which positive controllability is satisfied for SW poses. By considering two case study simulations, Section 5 demonstrates the use of the new metrics. Finally, Section 6 concludes the paper and presents areas of future work.

2. Background on Wrench Set Analysis

The dynamics of a CDR with d degrees-of-freedom actuated by m cables, as shown in Figure 1, can be expressed in the form

$$M(\mathbf{q})\ddot{\mathbf{q}} + \mathbf{C}(\mathbf{q}, \dot{\mathbf{q}}) + \mathbf{G}(\mathbf{q}) + \mathbf{w}_{\text{ext}} = -L^T(\mathbf{q})\mathbf{f}, \quad (1)$$

where $\mathbf{q} \in \mathbb{R}^d$ is the generalised coordinates (*pose*), $\mathbf{f} = [f_1 \ \dots \ f_m]^T \in \mathbb{R}^m$ is the cable force vector, $M \in \mathbb{R}^{d \times d}$ is the symmetric positive definite mass-inertia matrix, $\mathbf{C} \in \mathbb{R}^d$ is the Coriolis/centrifugal force vector, $\mathbf{G} \in \mathbb{R}^d$ is the gravitational force vector, $\mathbf{w}_{\text{ext}} \in \mathbb{R}^d$ is the external wrench vector and $L \in \mathbb{R}^{m \times d}$ is the Jacobian matrix. The positive cable force constraint can be expressed as

$$\mathbf{0} \leq \underline{\mathbf{f}} \leq \mathbf{f} \leq \bar{\mathbf{f}}, \quad (2)$$

where the bounds $\underline{\mathbf{f}}, \bar{\mathbf{f}} \in \mathbb{R}^m$ represent the minimum cable force necessary to overcome slack in the cables and the maximum allowable cable forces for safe operation, respectively^a. Cable characteristics such as cable mass and/or cable stiffness can be incorporated into the bounds $\underline{\mathbf{f}}$ and $\bar{\mathbf{f}}$. This may result in pose dependent bounds on the possible cable forces.

At a given pose, the available wrench set is defined as the set of wrenches that the CDR can produce. Using the Jacobian matrix L and the constraint (2), the available wrench set can be expressed as

$$\mathcal{W}_a(\mathbf{q}) = \{ \mathbf{w} \in \mathbb{R}^d : \mathbf{w} = -L^T(\mathbf{q})\mathbf{f}, \mathbf{f} \in [\underline{\mathbf{f}}, \bar{\mathbf{f}}] \}. \quad (3)$$

Due to the linear form of (3), the available wrench set $\mathcal{W}_a(\mathbf{q})$ possesses the shape of a special class of polytope known as a *zonotope*[13]. A pose \mathbf{q} satisfies the wrench-feasibility condition [12, 32] if the set of all desired wrenches $\mathcal{W}_d(\mathbf{q})$ is contained within the available wrench set $\mathcal{W}_a(\mathbf{q})$ such that

$$\mathcal{W}_d(\mathbf{q}) \subseteq \mathcal{W}_a(\mathbf{q}). \quad (4)$$

^aThe notation $\underline{\mathbf{f}} \leq \mathbf{f} \leq \bar{\mathbf{f}}$ indicates a component wise inequality such that $\underline{f}_i \leq f_i \leq \bar{f}_i, \forall i \in \{1, \dots, m\}$.

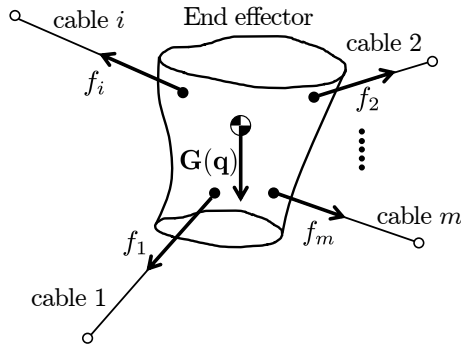


Figure 1: General Cable Driven Robot

The wrench-feasibility condition (4) is a general condition that can be used in the definition and evaluation of various other workspace conditions [13, 14]. For example, the wrench-closure condition can be defined using (4), where $\mathcal{W}_d = \mathbb{R}^n$ and the available wrench set is generated by (3) with $\underline{\mathbf{f}} = \mathbf{0}$ and $\bar{\mathbf{f}}$ set to infinity. Additionally, the static workspace condition can be defined with $\mathcal{W}_d = \mathbf{G}(\mathbf{q})$.

The relationship between $\mathcal{W}_d(\mathbf{q})$ and $\mathcal{W}_a(\mathbf{q})$ has been used to study the robustness and/or quality of the CDR capability [17, 14, 33]. One example of such a metric is the *capacity margin*. This metric has been used as a measure of how robustly a desired workspace condition is satisfied [14]. The measure corresponds to the minimum distance between $\mathcal{W}_d(\mathbf{q})$ and $\mathcal{W}_a(\mathbf{q})$ and is mathematically defined as

$$s(\mathbf{q}) = \min_{j=1,\dots,p} \left(\min_{k=1,\dots,l} s_{(j,k)}(\mathbf{q}) \right), \quad (5)$$

where the degree of constraint satisfaction $s_{(j,k)}(\mathbf{q})$ is the signed distance from the j th vertex of $\mathcal{W}_d(\mathbf{q})$ to the k th face of $\mathcal{W}_a(\mathbf{q})$ and p and l represent the number of vertices of $\mathcal{W}_d(\mathbf{q})$ and faces of $\mathcal{W}_a(\mathbf{q})$, respectively. The signed distance is defined such that if $s(\mathbf{q}) < 0$, then $\mathcal{W}_d(\mathbf{q}) \not\subseteq \mathcal{W}_a(\mathbf{q})$ and the robot is not capable of producing the desired wrench set at pose \mathbf{q} . If $s(\mathbf{q}) = 0$, the boundaries of the sets intersect, and the satisfaction of $\mathcal{W}_d(\mathbf{q}) \subseteq \mathcal{W}_a(\mathbf{q})$ is not robust to disturbances. If $s(\mathbf{q}) > 0$, then the desired wrench set can be produced at pose \mathbf{q} and at that pose the system is robust to additional external wrenches provided that $\|\mathbf{w}_{\text{ext}}\| \leq s(\mathbf{q})$.

3. Available Acceleration Set and the Acceleration Capability Measure

The analysis of motion generation requires consideration of the system's ability to produce joint acceleration and velocity. The wrench based tools presented in Section 2 could be used to consider these terms through the use of the equation of motion (1). Due to the nonlinearity of this equation, its use typically requires the explicit knowledge of the mechanism's trajectories in advance. This requirement confines any subsequent motion generation analysis to the understanding of the ability to produce defined trajectories rather than the ability to generate any arbitrary path and trajectory. Furthermore, while acceleration is related to wrench through the inversion of the inertia matrix, metrics on the wrench set are not always proportionally related to an acceleration space equivalent. This result means that wrench based metrics such as capacity margin cannot be used directly to infer the ability to generate kinematics and hence are not accurate measures for motion generation capability.

In this section, acceleration set analysis will be considered in place of wrench set analysis to gain an understanding of the ability to generate arbitrary motion. Section 3.1 introduces the available acceleration set and shows that analysis of the capability to produce acceleration cannot be observed from wrench based

measures such as the capacity margin. Section 3.2 then defines the *acceleration capability measure* as a workspace metric which evaluates the distance between sets in the acceleration space. Finally, Section 3.3 shows that analysis of the acceleration capability measure at static equilibrium can be used to obtain a trajectory independent measure of motion generation capability.

3.1. Available Acceleration Set

From the CDR equations of motion (1) and the wrench set definition (3), the wrench set $\mathcal{W}_a(\mathbf{q})$ can be used to determine the allowable joint velocities and accelerations at a known pose \mathbf{q} . Through (1), the desired wrench set $\mathcal{W}_d(\mathbf{q})$ can also be viewed as a set of desired $\dot{\mathbf{q}}$, $\ddot{\mathbf{q}}$ and \mathbf{w}_{ext} to be produced. For each fixed pose \mathbf{q} , with known $\dot{\mathbf{q}}$ and \mathbf{w}_{ext} , the capacity margin $s(\mathbf{q})$ therefore represents the magnitude of the term $M(\mathbf{q})\ddot{\mathbf{q}}$ that can be produced by the system. As a result, the capacity margin (5) can be used to approximate the maximum joint acceleration $\|\ddot{\mathbf{q}}\|$ that the CDR is capable of producing in all directions (*acceleration capability*). The bounds for the maximum joint acceleration can be expressed as

$$\sigma_{\min}(M^{-1}(\mathbf{q}))s(\mathbf{q}) \leq \|\ddot{\mathbf{q}}\| \leq \sigma_{\max}(M^{-1}(\mathbf{q}))s(\mathbf{q}), \quad (6)$$

where $\sigma_{\min}(M^{-1}(\mathbf{q}))$ and $\sigma_{\max}(M^{-1}(\mathbf{q}))$ represent the minimum and maximum singular values of the matrix $M^{-1}(\mathbf{q})$, respectively. From (6) and the interpretation that $\mathcal{W}_d(\mathbf{q})$ represents a set of desired $\dot{\mathbf{q}}$ and \mathbf{w}_{ext} , kinematic limitations for the magnitude of the joint acceleration $\|\ddot{\mathbf{q}}\|$ are estimated.

The inequality (6) only provides an estimate on the mechanism's true acceleration capability. As such, the available wrench set that has typically been applied for analysis of system kinetics [14, 13, 12], is ill suited for motion generation analysis. Compared with the estimated acceleration capability (6), the true acceleration capability should be used in the study of motion generation. Analogous to the wrench set $\mathcal{W}_a(\mathbf{q})$, the *available acceleration set* $\mathcal{A}_a(\mathbf{q}, \dot{\mathbf{q}})$ can be defined as the set of all accelerations that the CDR can produce at a given \mathbf{q} , $\dot{\mathbf{q}}$ and \mathbf{w}_{ext} . Without loss of generality, it will be assumed that no external wrenches act on the system such that $\mathbf{w}_{\text{ext}} = \mathbf{0}$ ^b. As such, the available acceleration set $\mathcal{A}_a(\mathbf{q}, \dot{\mathbf{q}})$ for the system (1) can be defined as

$$\mathcal{A}_a(\mathbf{q}, \dot{\mathbf{q}}) = \{\mathbf{a} \in \mathbb{R}^d : \mathbf{a} = -\mathcal{L}^T \mathbf{f} - \mathcal{C} - \mathcal{G}, \mathbf{f} \in [\underline{\mathbf{f}}, \bar{\mathbf{f}}]\}, \quad (7)$$

where $\mathcal{L}(\mathbf{q}) = L(\mathbf{q})M^{-1}(\mathbf{q})^c$, $\mathcal{C}(\mathbf{q}, \dot{\mathbf{q}}) = M^{-1}(\mathbf{q})\mathbf{C}(\mathbf{q}, \dot{\mathbf{q}})$ and $\mathcal{G}(\mathbf{q}) = M^{-1}(\mathbf{q})\mathbf{G}(\mathbf{q})$.

Figure 2 shows an example of the relationship between the sets $\mathcal{W}_a(\mathbf{q})$ and $\mathcal{A}_a(\mathbf{q}, \dot{\mathbf{q}})$ for a given pose \mathbf{q} , where the numbers indicate the corresponding edges of the sets within the wrench and acceleration spaces and the sets are consistent with acceleration and wrench sets that could be obtained for a 2 DoF 4 cable manipulator. For a given \mathbf{q} and $\dot{\mathbf{q}}$, the mapping between $\mathcal{W}_a(\mathbf{q})$ and $\mathcal{A}_a(\mathbf{q}, \dot{\mathbf{q}})$ consists of a translation due to gravitational and centrifugal/Coriolis forces as well as a matrix multiplication. As a result, $\mathcal{A}_a(\mathbf{q}, \dot{\mathbf{q}})$ is also a translated zonotope that possesses the same number of vertices and edges as $\mathcal{W}_a(\mathbf{q})$, where the centre is located at $\mathbf{a}_c = -\mathcal{C} - \mathcal{G}$.

An important artefact of the generalised inertia multiplication used in the mapping between $\mathcal{W}_a(\mathbf{q})$ and $\mathcal{A}_a(\mathbf{q}, \dot{\mathbf{q}})$ is that the closest face used in the calculation of the capacity margin (5) may not be the closest face to the corresponding point in the acceleration space, as a result of the different inertias associated with each link. For example, in Figure 2 the point $\mathbf{C}(\mathbf{q}, \dot{\mathbf{q}}) + \mathbf{G}(\mathbf{q})$ is closest to edge 1, whereas the corresponding point in the acceleration space ($\mathbf{a} = \mathbf{0}$) is closest to edge 6. This means that, the capacity margin s is not linearly related to acceleration capability. This effect explains the approximating nature of (6) with the true acceleration capability. Therefore, it is more appropriate to analyse motion generation using the available acceleration set (7) compared with the capacity margin, since it provides direct information about the motion generation capabilities of the CDR.

^bNon-zero \mathbf{w}_{ext} can be considered as a translation acting on the available acceleration set. If $\|\mathbf{w}_{\text{ext}}\| \leq w$ then the set distance measures developed in the subsequent sections can consider unknown external wrench by suitable contraction of \mathcal{A}_a by radius w .

^c $\mathcal{L}(\mathbf{q})$ is defined such that $\mathcal{L}^T(\mathbf{q}) = M^{-1}(\mathbf{q})L^T(\mathbf{q})$. This means that $\mathcal{L}(\mathbf{q}) = L(\mathbf{q})M^{-T}(\mathbf{q}) = L(\mathbf{q})M^{-1}(\mathbf{q})$, since $M(\mathbf{q})$ is symmetric and positive definite.

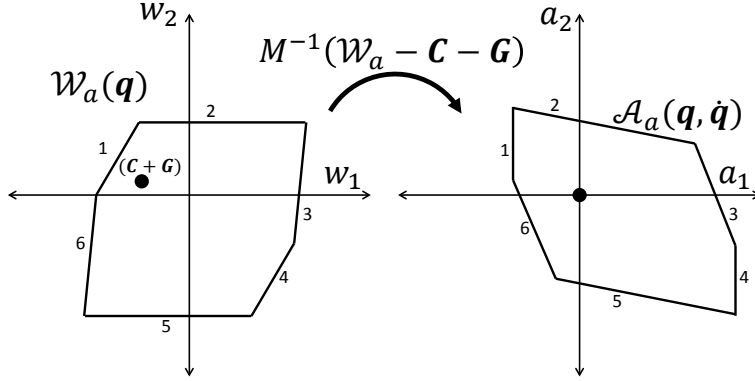


Figure 2: Available Wrench and Acceleration Sets

Since the available acceleration set $\mathcal{A}_a(\mathbf{q}, \dot{\mathbf{q}})$ is a polytope, it can be mathematically described by a set of q linear inequalities in the form $D\mathbf{a} \leq \mathbf{e}$, where $\mathbf{a} \in \mathbb{R}^d$, $D \in \mathbb{R}^{q \times d}$ and $\mathbf{e} \in \mathbb{R}^q$. Like the available wrench set, the available acceleration set requires a linear inequality for each face of $\mathcal{A}_a(\mathbf{q}, \dot{\mathbf{q}})$ [14]. This limits the practicality of using $\mathcal{A}_a(\mathbf{q}, \dot{\mathbf{q}})$ for online analysis of motion generation capability, whereby a unique description of the zonotope may be required for every candidate state of the manipulator.

3.2. Acceleration Capability Measure

In a similar manner to wrench space analysis, workspace conditions can be defined for acceleration analysis by considering the relationship between a *desired acceleration set* $\mathcal{A}_d(\mathbf{q}, \dot{\mathbf{q}})$ and the available acceleration set $\mathcal{A}_a(\mathbf{q}, \dot{\mathbf{q}})$. To analyse this relationship, let the *acceleration capability measure*^d (ACM) be defined as the acceleration space equivalent of the capacity margin

$$\rho(\mathbf{q}, \dot{\mathbf{q}}) = \min_{j=1, \dots, p} \left(\min_{k=1, \dots, l} \rho_{(j,k)}(\mathbf{q}, \dot{\mathbf{q}}) \right), \quad (8)$$

where the degree of constraint satisfaction $\rho_{(j,k)}(\mathbf{q}, \dot{\mathbf{q}})$ is the signed distance from the j th vertex of $\mathcal{A}_d(\mathbf{q}, \dot{\mathbf{q}})$ to the k th face of $\mathcal{A}_a(\mathbf{q}, \dot{\mathbf{q}})$. Figure 3 shows a graphical representation of the acceleration capability measure for a given $\mathcal{A}_d(\mathbf{q}, \dot{\mathbf{q}})$, $\mathcal{A}_a(\mathbf{q}, \dot{\mathbf{q}})$, \mathbf{q} and $\dot{\mathbf{q}}$. It can be seen that for fixed \mathbf{q} and $\dot{\mathbf{q}}$, the manipulator possesses the capability to produce the $\mathcal{A}_d(\mathbf{q}, \dot{\mathbf{q}})$ and the ACM then quantifies the capability of the CDR to produce additional joint accelerations. Furthermore, the signs of $\rho(\mathbf{q}, \dot{\mathbf{q}})$ and $s(\mathbf{q})$ have analogous meaning. That is, if $\rho(\mathbf{q}, \dot{\mathbf{q}}) > 0$, then the desired acceleration set can be produced and there is capability to produce an additional acceleration $\bar{\mathbf{a}} \in \mathbb{R}^d$, provided that $\|\bar{\mathbf{a}}\| \leq \rho(\mathbf{q}, \dot{\mathbf{q}})$. Unlike the capacity margin, the acceleration capability $\rho(\mathbf{q}, \dot{\mathbf{q}})$ is a function of both \mathbf{q} and $\dot{\mathbf{q}}$. As such, the additional acceleration that can be produced in all directions changes with joint velocity, which complicates the analysis of the ACM when compared to that of the capacity margin. A joint velocity independent approximation of this measure will be considered in the subsection that follows.

3.3. Static Equilibrium Acceleration Capability Measure

The ability to maintain static equilibrium (*SE*) is important and commonly considered in the study of CDRs [34, 5]. To aid in the analysis of the manipulator's capability from static equilibrium, the static

^dFor simplicity of presentation, in this paper the ACM is presented for the case of dimensionally homogeneous units. In the case of non-dimensionally homogeneous units the Jacobian matrix can be altered in a manner consistent with Section 2 of [14].

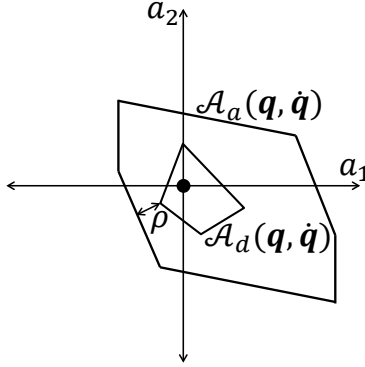


Figure 3: Example of the Acceleration Capability Measure

equilibrium acceleration capability measure (*SEACM*) $\varrho(\mathbf{q})$ is defined as the measure of the CDR's capability to produce acceleration from SE. This means that the SEACM represents a special case of the ACM in which

$$\varrho(\mathbf{q}) = \rho(\mathbf{q}, \mathbf{0}), \quad \mathcal{A}_d = \{\mathbf{0}\}. \quad (9)$$

Since the only $\dot{\mathbf{q}}$ dependent term in (7) is the Coriolis and Centrifugal term $\mathbf{C}(\mathbf{q}, \dot{\mathbf{q}})$, knowledge of the SEACM can also be used to approximate $\rho(\mathbf{q}, \dot{\mathbf{q}})$ provided that a bound on $\|\mathbf{C}(\mathbf{q}, \dot{\mathbf{q}})\|$ is known. Such an approximation would simplify the analysis of motion generation such that speed and acceleration limits for the CDR can be determined. This is because the SEACM can be evaluated without the need for the trajectory to be prescribed a priori. When compared with motion generation analysis using the ACM, this approach therefore does not require a search through the set of possible motions.

By definition (9), the SEACM represents the minimum distance from $\mathcal{A}_d = \mathbf{0}$ to $\mathcal{A}_a(\mathbf{q}, \dot{\mathbf{q}})$ for the case when $\dot{\mathbf{q}} = \mathbf{0}$. In contrast, when $\mathcal{A}_d = \mathbf{0}$, the ACM (8) represents the minimum distance from $\mathbf{0}$ to $\mathcal{A}_a(\mathbf{q}, \dot{\mathbf{q}})$ for the given $\dot{\mathbf{q}}$. $\mathbf{C}(\mathbf{q}, \dot{\mathbf{q}})$ is the only $\dot{\mathbf{q}}$ dependent term used in generating \mathcal{A}_a . Since this term represents a translation acting on the entire set $\mathcal{A}_a(\mathbf{q}, \mathbf{0})$, the following condition can be used to provide a sufficient condition for positive ACM:

Condition 1. $\rho(\mathbf{q}, \dot{\mathbf{q}}) \geq 0$ if $\|\mathbf{C}(\mathbf{q}, \dot{\mathbf{q}})\| \leq \varrho(\mathbf{q})$.

To evaluate how $\|\mathbf{C}(\mathbf{q}, \dot{\mathbf{q}})\|$ changes as a function of $\dot{\mathbf{q}}$, it is noted that the term $\mathbf{C}(\mathbf{q}, \dot{\mathbf{q}})$ has a quadratic relationship with $\dot{\mathbf{q}}$. This means that $\mathbf{C}(\mathbf{q}, \dot{\mathbf{q}})$ and $\mathbf{C}(\mathbf{q}, \dot{\mathbf{q}})$ can be represented in the forms

$$\mathbf{C}(\mathbf{q}, \dot{\mathbf{q}}) = \begin{bmatrix} \dot{\mathbf{q}}^T N_1(\mathbf{q}) \dot{\mathbf{q}} \\ \vdots \\ \dot{\mathbf{q}}^T N_d(\mathbf{q}) \dot{\mathbf{q}} \end{bmatrix}, \quad \mathbf{C}(\mathbf{q}, \dot{\mathbf{q}}) = \begin{bmatrix} \dot{\mathbf{q}}^T P_1(\mathbf{q}) \dot{\mathbf{q}} \\ \vdots \\ \dot{\mathbf{q}}^T P_d(\mathbf{q}) \dot{\mathbf{q}} \end{bmatrix}, \quad (10)$$

where $N_i \in \mathbb{R}^{d \times d} \forall i \in \{1, \dots, d\}$ and $P_i(\mathbf{q}) = \sum_{j=1}^d \left((M^{-1}(\mathbf{q}))_{ij} N_j \right)$ with $(M^{-1}(\mathbf{q}))_{ij}$ referring to the element at the i th row and j th column of the matrix $(M^{-1}(\mathbf{q}))$. Since it is known that there exists a scalar function $\mu(\mathbf{q})$ such that $\|\mathbf{C}(\mathbf{q}, \dot{\mathbf{q}})\| \leq \mu(\mathbf{q}) \|\dot{\mathbf{q}}\|^2$ [35], a scalar function $\kappa(\mathbf{q})^e$ can always be found such that

$$\|\mathbf{C}(\mathbf{q}, \dot{\mathbf{q}})\| \leq \kappa(\mathbf{q}) \|\dot{\mathbf{q}}\|^2. \quad (11)$$

Condition 1 provides a bound on how large the magnitude of $\mathbf{C}(\mathbf{q}, \dot{\mathbf{q}})$ can be such that the CDR possesses non-negative acceleration capability. Inequality (11) then provides a worst case bound on how the magnitude

^eThere are multiple different methods that can be utilised to compute the scalar functions $\mu(\mathbf{q})$ and $\kappa(\mathbf{q})$ [35]. One example method of computation for $\kappa(\mathbf{q})$ is provided in Section 4.2

of $\mathcal{C}(\mathbf{q}, \dot{\mathbf{q}})$ varies as a function of the joint speed $\|\dot{\mathbf{q}}\|$. Using these two results, $\varrho(\mathbf{q})$ and $\kappa(\mathbf{q})$ can be used to obtain a bound on $\rho(\mathbf{q}, \dot{\mathbf{q}})$ as a function of $\|\dot{\mathbf{q}}\|$ such that the trajectory need not be known a priori. Here by definition $\rho(\mathbf{q}, \mathbf{0}) = \varrho(\mathbf{q})$ and using the reasoning Condition 1, $\rho(\mathbf{q}, \dot{\mathbf{q}})$ must be greater than the worst case translation which corresponds to a translation of $\kappa(\mathbf{q})\|\dot{\mathbf{q}}\|^2$ using (11). As a result, the SEACM can therefore be related to the ACM in the case where $\mathcal{A}_d(\mathbf{q}, \dot{\mathbf{q}}) = \mathbf{0}$ through the inequality

$$\rho(\mathbf{q}, \dot{\mathbf{q}}) \geq \varrho(\mathbf{q}) - \kappa(\mathbf{q})\|\dot{\mathbf{q}}\|^2. \quad (12)$$

From (12), the ACM $\rho(\mathbf{q}, \dot{\mathbf{q}})$ is therefore non-negative if

$$\varrho(\mathbf{q}) - \kappa(\mathbf{q})\|\dot{\mathbf{q}}\|^2 \geq 0. \quad (13)$$

This means that the CDR always possesses the capability to produce acceleration in all directions provided that

$$\|\dot{\mathbf{q}}\| < \sqrt{\frac{\varrho(\mathbf{q})}{\kappa(\mathbf{q})}}. \quad (14)$$

Inequality (12) can also be used as an estimation of the magnitude of the acceleration that can be produced for any known robot speed. Defining the *capability hypersphere* to be the set of accelerations

$$\mathcal{A}_a^{\varrho}(\mathbf{q}) = \{\mathbf{a} \in \mathbb{R}^d : \|\mathbf{a}\| \leq \varrho(\mathbf{q})\}, \quad (15)$$

(12) shows that ρ is the distance between the surface of $\mathcal{A}_a^{\varrho}(\mathbf{q})$ and the hypersphere that bounds the translation $\mathcal{C}(\mathbf{q}, \dot{\mathbf{q}})$.

Figure 4 shows the SEACM and the corresponding capability hypersphere (15) for the example acceleration set. It can be seen that the capability hypersphere represents the largest hypersphere of acceleration that is contained within $\mathcal{A}_a(\mathbf{q}, \dot{\mathbf{q}})$ and has a centre at $\ddot{\mathbf{q}} = \mathbf{0}$. The advantage of this representation is that the capability hypersphere can be expressed using a single variable ϱ which has a more intuitive physical meaning when compared with the inequalities necessary in describing the zonotope $\mathcal{A}_a(\mathbf{q}, \dot{\mathbf{q}})$. Furthermore, the capability hypersphere allows for the velocity of the CDR to be considered independent of its direction through (12). From this, kinematic limits on both speed and acceleration can be obtained without the need to search through the acceleration set.

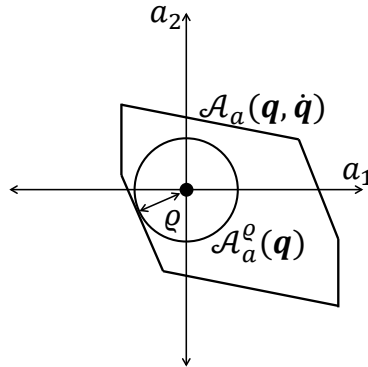


Figure 4: Example of the SEACM and capability hypersphere

4. Motion Generation within the Static Workspace

In this section, the ACM will be used to gain an understanding of the motion generation capability of poses within the static workspace (SW) at non-zero joint velocity. The positive controllability condition is

first reviewed and applied in order to present a rigorous proof that poses within the SW can be used for motion generation. Using this result, the *maximum controllable speed* metric is then introduced as a new workspace metric which estimates the speed capabilities of the CDR under consideration.

4.1. Static Workspace and Positive Controllability

Consider a nonlinear time invariant system given modelled by

$$\dot{\mathbf{x}} = f(\mathbf{x}, \mathbf{u}), \quad \mathbf{x}(0) = \mathbf{x}_0, \quad (16)$$

where $\mathbf{x} \in \mathbb{R}^n$ represents the n -dimensional state and $\mathbf{u} \in \mathbb{R}^m$. The system (16) is said to be *positive controllable* if for all $\mathbf{x}_0, \mathbf{x}_f \in \mathbb{R}^n$, there exists a finite time T and a non-negative control input sequence $\mathbf{u}(t) \geq \mathbf{0}$, $\forall 0 \leq t \leq T$, which will bring the system from $\mathbf{x}(0) = \mathbf{x}_0$ to $\mathbf{x}(T) = \mathbf{x}_f$ [28]. A *region* $\mathcal{D} \subseteq \mathbb{R}^n$ is positive controllable if for all states $\mathbf{x}_0, \mathbf{x}_f \in \mathcal{D}$, the positive controllability condition is satisfied. If a state lies in the interior of a positive controllable region, then the state is *locally positive controllable*. Local positive controllability can be evaluated without knowledge of the positive controllable regions using techniques such as linearisation[29].

Using the local positive controllability theory presented above, the following results is obtained to construct approximate regions of positive controllability.

Theorem 1. *If a set of states are locally positive controllable and connected^f, then the set forms a positive controllable region.*

Proof. See Appendix A. □

Positive controllability can be studied for CDRs by representing the system in state space form where $\mathbf{x} = [\mathbf{q}^T \quad \dot{\mathbf{q}}^T]^T$ and $\mathbf{u} = \mathbf{f}$. Using this state representation, satisfaction of the positive controllability condition corresponds to the capability to connect any two joint poses and velocities. As such, positive controllability provides a sufficient condition on the feasibility of motion generation which is defined to consider the problem of connecting two joint poses. For CDRs, positive controllability is related to the SEACM introduced in Section 3 through Theorem 2:

Theorem 2. *If a pose \mathbf{q}^* has a positive SEACM, then it is locally positive controllable at the static equilibrium state $[\mathbf{q}^{*T} \quad \mathbf{0}^T]^T$.*

Proof. See Appendix B. □

Using Theorem 2, the *positive controllable workspace* (PCW) can be defined as the set

$$PCW = \{\mathbf{q} \in \mathbb{R}^d : \varrho(\mathbf{q}) > 0\}. \quad (17)$$

From the workspace interpretation presented in Section 3.1, it can be seen that an alternative definition of the SW is the set

$$SW = \{\mathbf{q} \in \mathbb{R}^d : \varrho(\mathbf{q}) \geq 0\}. \quad (18)$$

The PCW therefore represents a subset of the SW which is robust to external disturbances and/or uncertainties. This workspace can also be used with Theorem 1 to identify regions of positive controllability within the state space.

The use of Theorems 1 and 2 shows that the SW can be used for motion generation. Since Theorem 2 is only applicable to some neighbourhood of a static equilibrium, it only considers regions of positive controllability with suitably small joint velocities. This indicates that while the existence of these regions implies that a motion can be generated to connect the poses, there is no knowledge of the velocities that can be used in generating that motion. The problem of determining upper bounds on the velocities of these motions is considered in the subsection that follows.

^fA set is *connected* if it cannot be represented as the union of two disjoint, non-empty, open sets [36]

4.2. Speed Capabilities of the Static Workspace

By definition, CDR states within a positive controllable region can be connected by a non-negative control input. The PCW generated regions can therefore be extended to consider $\dot{\mathbf{q}} \neq \mathbf{0}$ by finding the velocities for which the CDR can be brought back to static equilibrium. Using (12), it will be shown that it is possible to obtain a conservative estimate of the maximum speed $V_{max}(\mathbf{q})$ such that for all $\|\dot{\mathbf{q}}\| \leq V_{max}(\mathbf{q})$ the CDR can return to static equilibrium (*maximum controllable speed*). The consideration of $V_{max}(\mathbf{q})$ in place of $\dot{\mathbf{q}}$ simplifies the analysis and allows the positive controllable region to be stored using the static workspace and a single metric.

In this work, a numerical approach will be adopted where the maximum controllable speed (MCS) in stopping at a known distance r from \mathbf{q} will be bounded. This bound will be obtained by considering the worst possible acceleration capability of the mechanism over the set $\mathcal{B}(\mathbf{q}, r)$ where

$$\mathcal{B}(\mathbf{q}, r) = \{\mathbf{q}^\circ \in \mathbb{R}^d : \|\mathbf{q}^\circ - \mathbf{q}\| \leq r\}. \quad (19)$$

The use of this bound results in a conservative estimate of the MCS which can be determined independently of the direction of velocity such that a trajectory dependent search is not required.

Using the well known constant acceleration formula

$$V_{max}^2(\mathbf{q}) = 2a_{max}(\mathbf{q})r, \quad (20)$$

a bound on the MCS can be determined by solving for a_{max} which represents an estimate on the maximum constant acceleration produced over the set $\mathcal{B}(\mathbf{q}, r)$ (19). As discussed in Section 3, the ACM represents the maximum acceleration that can be produced in all directions for a known \mathbf{q} and $\|\dot{\mathbf{q}}\|$. From (12), an estimate $\hat{\rho}(\mathbf{q}, \dot{\mathbf{q}})$ of the ACM is given by

$$\hat{\rho}(\mathbf{q}, \dot{\mathbf{q}}) = \varrho(\mathbf{q}) - \kappa(\mathbf{q})\|\dot{\mathbf{q}}\|^2, \quad (21)$$

where using (10) one possible bounding scalar function $\kappa(\mathbf{q})$ for (11) is given by $\kappa(\mathbf{q}) = \sqrt{\sum_{i=1}^d (\sigma_{max}(P_i(\mathbf{q})))^2}$, since

$$\|\mathbf{C}(\mathbf{q}, \dot{\mathbf{q}})\| = \sqrt{\sum_{i=1}^d (\dot{\mathbf{q}}^T P_i \dot{\mathbf{q}})^T (\dot{\mathbf{q}}^T P_i \dot{\mathbf{q}})} \leq \|\dot{\mathbf{q}}\|^2 \sqrt{\sum_{i=1}^d (\sigma_{max}(P_i))^2}. \quad (22)$$

The maximum acceleration is therefore estimated by finding the maximum value that $\hat{\rho}(\mathbf{q}, \dot{\mathbf{q}})$ takes over $\mathcal{B}(\mathbf{q}, r)$. This value is estimated by setting $\|\dot{\mathbf{q}}\|$ at its maximum value V_{max} and letting ϱ and κ be fixed to their minimum and maximum values over the interval, given by ϱ_{min} and κ_{max} respectively. This results in the choice of a_{max} as

$$a_{max}(\mathbf{q}) = \varrho_{min}(\mathbf{q}) - \kappa_{max}(\mathbf{q})V_{max}^2. \quad (23)$$

Substituting the expression for a_{max} (23) into the expression for V_{max} (20), the MCS is conservatively estimated over $\mathcal{B}(\mathbf{q}, r)$ as

$$V_{max}(\mathbf{q}) = \sqrt{\frac{2\varrho_{min}(\mathbf{q})r}{1 + 2\kappa_{max}(\mathbf{q})r}}. \quad (24)$$

Equation (24) computes the MCS under the assumption that the distance to rest r is fixed. To account for an unknown r , Algorithm 1 is proposed, where $\mathbf{q} \in \mathbb{R}^d$ is a given pose and i_{max} is the maximum number of iteration allowed in computing the solution.

Algorithm 1 represents a means of approximating the MCS for a given pose. Without the MCS, the positive controllable regions obtained in Section 4.1 cannot be used in generating motion. This is because knowledge of the MCS allows for the positive controllable regions to be extended to consider non-zero joint velocity. Using the resulting regions, motion generation capability can be analysed using the acceleration limits from Section 3.

Algorithm 1 Iterative Method for Determining V_{max}

```
while ( $i \leq i_{max}$ ) do  
   $r \leftarrow r + i\delta\mathbf{q}$ , where  $\delta\mathbf{q}$  is the constant sample size.  
   $\varrho_{min}(\mathbf{q}) \leftarrow \min_{\mathbf{q} \in \mathcal{B}(\mathbf{q}, r)} \varrho(\mathbf{q})$ .  
   $\kappa_{max}(\mathbf{q}) \leftarrow \max_{\mathbf{q} \in \mathcal{B}(\mathbf{q}, r)} \kappa(\mathbf{q})$ .  
   $V_{max}(\mathbf{q}) \leftarrow \sqrt{\frac{2\varrho_{min}(\mathbf{q})r}{1+2\kappa_{max}(\mathbf{q})r}}$ .  
   $i \leftarrow i + 1$ .
```

5. Results and Discussion

5.1. Outline of Results

In this section, motion generation capability analysis will be considered through the application of the SEACM and MCS measures. These measures have been implemented in the CASPR platform [31] such that their analysis can be conveniently performed onto different CDRs. Two case study manipulators will be considered:

1. A 2 link Planar CDR,
2. A 6 DoF Spatial Cable Driven Parallel Robot (CDPR).

In each of the case studies, the SW will be generated and the value of the ACM and MCS computed throughout the entire workspace. In Case Study 1, this information will be analysed in order to gain greater insight into the motion generation capability across the workspace. This analysis will consist of an evaluation of the meaning of the metrics for path and trajectory planning. Case Study 2 will then investigate the results on a higher degree of freedom example.

Throughout the case studies, the resulting regions of operation obtained from the SW and MCS will be compared with those obtained from the wrench closure workspace. The WCW has not been previously used as a tool for motion generation analysis. However, due to its definition in the ability to generate any wrench and hence any acceleration, connected workspace regions are therefore controllable by definition. As a result, the WCW represents an idealised set for which all poses and joint velocities can be produced, making it an ideal point of comparison to the set of joint velocities and SW poses obtained by using the MCS.

The section will conclude by providing further discussion into the use of the metrics beyond that considered in the case studies. This will include a comparison of the insight that is provided by the metrics when compared to the application of trajectory planners as well as a discussion of the computational complexity of the proposed algorithm.

5.2. Kinematic Analysis of a 2 Link Planar CDR

Consider the 2 link planar CDR shown in Figure 5. The CDR is articulated by two revolute joints ($d = 2$) and is driven by four cables ($m = 4$). It is assumed that gravity acts in the $-y$ direction. Let the two rigid links be identical with a uniform distribution of mass $m_1 = m_2 = 1kg$ with lengths $\ell_1 = \ell_2 = 1m$. Furthermore, let the i th cable have cable mountings described by the base attachment vector \mathbf{r}_{OA_i} , which is a vector from the base point O to the attachment location A_i , and the rigid link attachment vector $\mathbf{r}_{G_j B_i}$, where G_j refers to the centre of gravity of the j th rigid link and B_i refers to the attachment point on rigid link j for cable i . Table 1 summarises the cable attachment information for the cable driven manipulator shown in Figure 5.

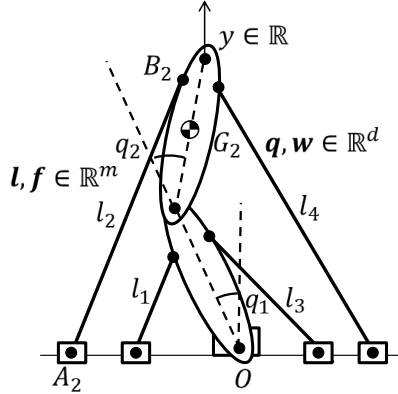


Figure 5: 2 Link Planar Cable Driven Manipulator

\mathbf{r}_{OA_1}	$[-0.5 \ 0]^T$	$\mathbf{r}_{G_1B_1}$	$[-0.1 \ 0.3]^T$
\mathbf{r}_{OA_2}	$[-1.5 \ 0]^T$	$\mathbf{r}_{G_2B_2}$	$[-0.1 \ 0.3]^T$
\mathbf{r}_{OA_3}	$[0.5 \ 0]^T$	$\mathbf{r}_{G_1B_3}$	$[0.1 \ 0.3]^T$
\mathbf{r}_{OA_4}	$[1.5 \ 0]^T$	$\mathbf{r}_{G_2B_4}$	$[0.1 \ 0.3]^T$

Table 1: Planar Manipulator Mechanism Parameters

5.2.1. Workspace Analysis

Figures 6a and 6b show the SW and WCW for this example system, where the SW was computed with cable force $0 \leq f_i \leq 250\text{N}$ for all $i \in \{1, \dots, 4\}$ and a uniform sampling of 1° was used in numerically generating the workspaces. From Figure 6a, it can be observed that the SW has a volume that represents of 87.1% of the total joint space volume. Furthermore, this workspace is comprised of a single connected region. In contrast, Figure 6b shows that the WCW consists of two disconnected regions that possess a total workspace coverage of only 67.4%.

By Theorems 1 and 2, it can be seen in Figure 6a that the CDR is capable of generating motion between any two poses that are contained within the single connected component. This result demonstrates that regions of allowable operation obtained from the SW can increase the set of possible operating configurations both by increasing the number of poses in the workspace and by identifying otherwise unseen connectivity between workspace regions. However, the use of the SW on its own does not consider the joint velocities at which motions can be generated. The SW therefore on its own provides an incomplete picture of the CDR's motion generation capability. Particularly, this is with regards to the speeds at which certain motions can be achieved and to which regions of the workspace are more favourable in terms of speed and robustness in the generation of arbitrary motion.

5.2.2. Acceleration Set Analysis

The acceleration set represents the set of all accelerations that can be produced by the CDR at a given pose. The set therefore indicates the capability of a mechanism to accelerate from rest and through (12) can also be used to approximate how capable the mechanism is in changing direction and/or speed during a motion. Figures 7a and 7b show the available acceleration sets at static equilibrium of this mechanism for two example poses: $\mathbf{q}_1 = [-30^\circ \ -15^\circ]^T$ and $\mathbf{q}_2 = [0^\circ \ 150^\circ]^T$, respectively. From the $\mathcal{A}_a^g(\mathbf{q})$ sets drawn in these figures, it can be seen that at pose \mathbf{q}_2 , the mechanism can produce 141.91 rad/s^2 of acceleration in all directions, making the CDR more capable than at pose \mathbf{q}_1 in which the mechanism can only produce 78.25 rad/s^2 . This higher acceleration indicates that it is more favourable for the mechanism to start motion at poses in the vicinity of \mathbf{q}_2 .

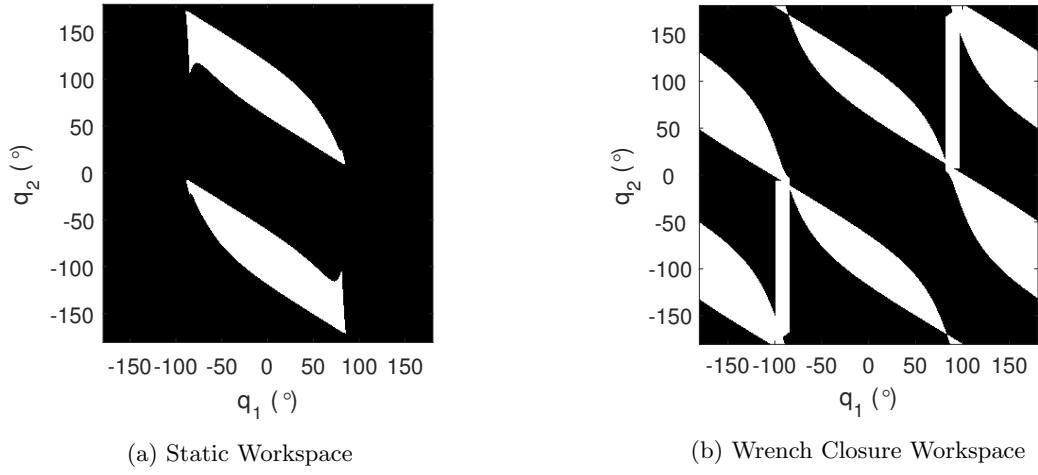


Figure 6: Static and Wrench Closure Workspaces of the 2 link planar manipulator

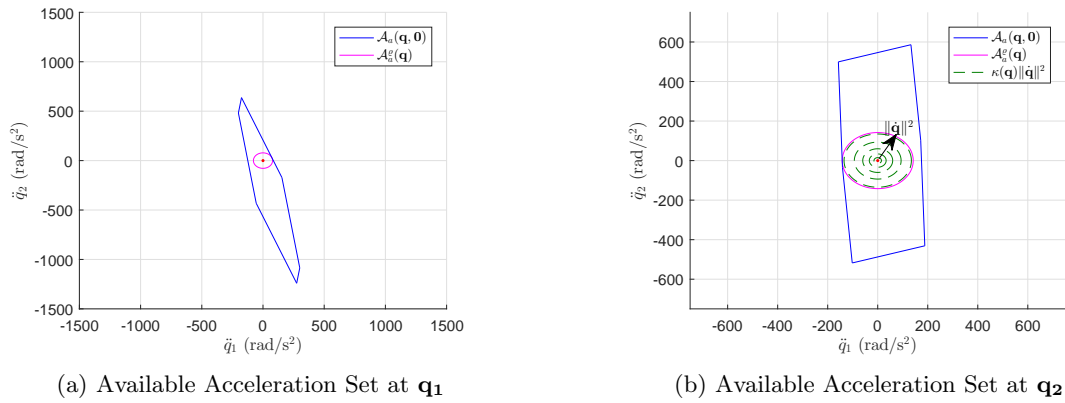


Figure 7: Available Acceleration Sets at Different Poses

Figures 7a and 7b also depict the capability hyperspheres (15) for each of the example poses. Although, these hyperspheres only represent a small fraction of the acceleration set volume, they provide the knowledge of the maximum magnitude of acceleration that can be produced in any direction. This means that the capability hypersphere can be used in combination with (12) to approximate the acceleration capability of the mechanism at a given pose and joint speed. This can be observed using the green dashed circles of Figure 7b that represent the possible worst case magnitudes of the vector $\mathcal{C}(\mathbf{q}, \dot{\mathbf{q}})$ obtained using the inequality (22). As such, the worst case acceleration that can be produced at a given $\|\dot{\mathbf{q}}\|$ then corresponds to the radial distance from the capability hypersphere boundary to the appropriate green dashed circle.

By performing the above analysis at every pose of the joint space, Figure 8 depicts the SEACM over all poses of the SW. From this figure, it can be observed that the acceleration capability of the manipulator ranges from zero at poses outside of or on the boundary of the SW to a maximum of 187.42 rad/s^2 at approximately $\mathbf{q} = [-139^\circ \quad -170^\circ]^T$. The changing magnitudes within the figure also indicate that the CDR is more capable of accelerating within different disjoint regions of the SW. This information can be used to evaluate different trajectories, such as Path 1 and Path 2 as shown in Figure 8. Particularly, the ACM indicates that it is possible for the mechanism to accelerate at larger magnitude for Path 2 then it is for Path 1. However, using (12), the ACM also indicates that the change in direction used in Path 2 may be difficult to achieve in practice, due to the limited capability to accelerate over a large region of the middle of the path. From this analysis, paths such as Path 1 can be identified as more desirable to be applied onto this CDR. This information can also be used to bias path planners to remain within such regions throughout operation.

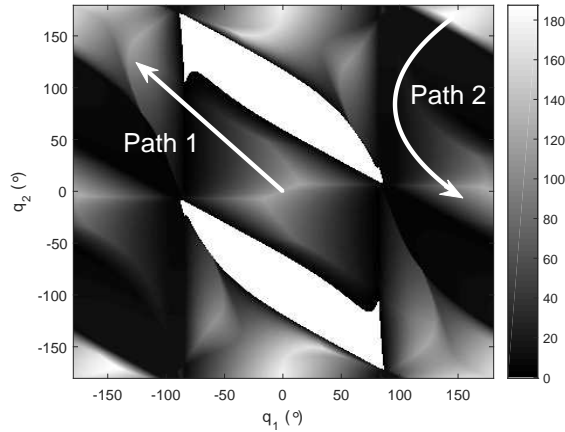


Figure 8: Static Equilibrium Acceleration Capability Measure $\rho(\mathbf{q})$ - It can be seen that Path 2 possesses higher initial capability to accelerate when compared to Path 1, however the path is limited to lower speed of operation due to the lower SEACM throughout the middle of the trajectory.

It should be noted, that the regions of high SEACM are all contained within disconnected components of the WCW. This is consistent with the intuition that within the WCW, the CDR is likely to be more capable in generating motion since the cable forces can produce accelerations larger than that of the gravitational force. However, this result does not hold over the entire WCW. This is due both to the practical cable force upper bounds not considered in wrench closure analysis and the proximity of certain poses to unilateral singularities [16].

5.2.3. Application of the ACM to Task Scaling

As a result of (12), the capability hypersphere and SEACM can be used to identify kinematic limits for task scaling. Consider the example paths shown in the Figure 8. For each path, all poses have non-zero SEACM. This means that a trajectory can be generated by the CDR to follow each of the desired paths. Furthermore at each pose of the path, Figure 9 depicts the estimate of the acceleration limits obtained using

(12) for each possible choice of speed. On this figure a desired trajectory corresponds to a curve in the path parameter and $\|\dot{\mathbf{q}}\|$, in which task scaling acts to scale the curve in the $\|\dot{\mathbf{q}}\|$ axis. A valid trajectory can therefore be identified by ensuring that the desired acceleration always remains within the non-negative component of $\|\dot{\mathbf{q}}\|$ as shown in the figure. In the case of task scaling this would correspond to identifying the minimum scale parameter such that for all path parameter values, the trajectory profile remains at joint speeds with non-zero acceleration capability.

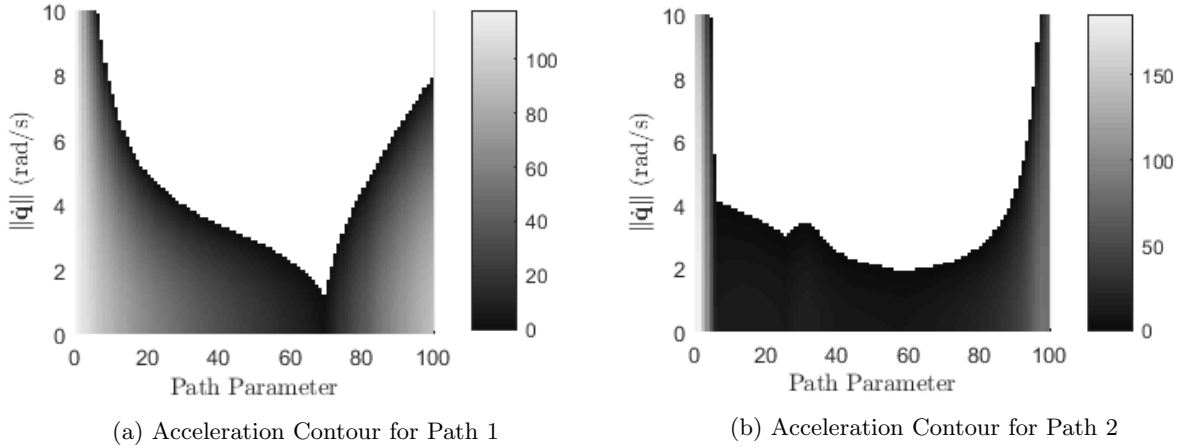


Figure 9: Acceleration Contours for the Desired Paths

5.2.4. The MCS and Path Evaluation

The MCS represents an estimate on the maximum speed at which the mechanism can be brought back to static equilibrium. As such, the MCS can be used in addition to the ACM in providing insight into the motion generation capability of the CDR. Figure 10 shows the MCS for the example mechanism. It can be seen that the relative magnitudes of the MCS follow a similar pattern to that of the SEACM. This indicates that the CDR is able to return to static equilibrium at higher speeds in the regions at which it has high acceleration capability at static equilibrium. Since this is the case, the operation of the mechanism should favour these regions wherever possible in order to maximise both the speed of operation and the robustness of the trajectory tracking.

Compared to the ACM, the regions of largest MCS are however larger than that of the regions of largest SEACM and the maximum value of 7.69 rad/s is instead found at approximately $\mathbf{q} = [0^\circ \ 180^\circ]^T$. This result is consistent with the filtering approach presented in Algorithm 1 and suggests that it is safer to use the CDR at higher speeds when it is closer to the centre of SW regions. The SEACM should however still be considered for sharp changes in paths, since the MCS does not explicitly measure the capability to produce acceleration.

The information contained within Figure 10 represents a conservative estimate of the maximum speed at which the CDR can be guaranteed to be able to return to static equilibrium. This means that if a motion satisfies the kinematic constraints, then it will be possible to connect back to a desired path and/or pose in the presence of disturbances. Figure 10 shows two possible trajectories that could be used to connect two desired poses and Figure 11 shows the specific MCS values over each of the paths with regards to a path parameter. It can be seen from Figure 11 that Path 2 is more favourable since it has larger MCS over nearly all of the path. This suggests that the CDR is more capable of generating motion throughout Path 2, resulting in a likely quicker time of execution and robustness (resulting from the SEACM over the corresponding region).

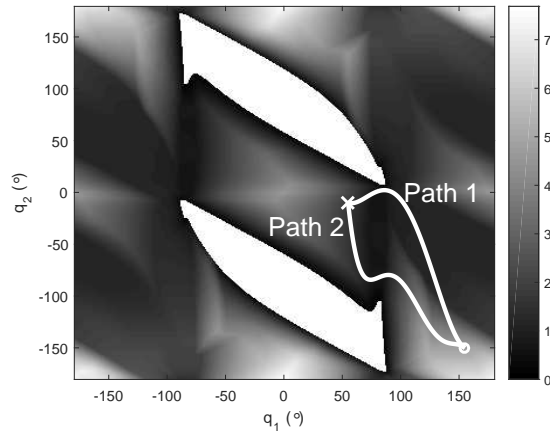


Figure 10: Maximum Controllable Speed Measure $V_{max}(\mathbf{q})$ - It can be seen that Path 2 possesses predominately higher MCS when compared to Path 1 indicating that this path can likely be executed at higher speed.

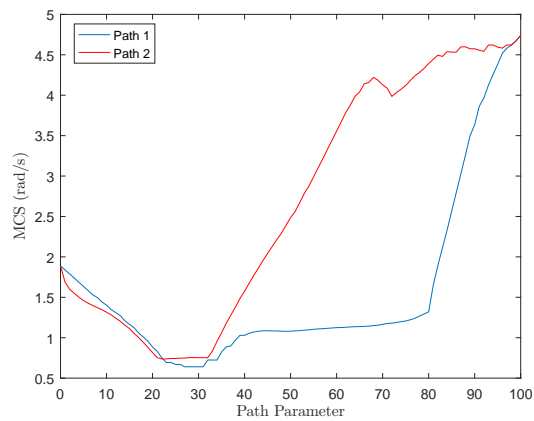


Figure 11: Comparison of MCS over Paths 1 and 2

5.3. Kinematic Analysis of a Spatial CDR

To show the application of the derived metrics to higher dimensional systems, consider the 6 DoF ($d = 6$) spatial manipulator shown in Figure 12. Let this CDR be driven by seven cable ($m = 7$) with cable attachments corresponding to those of [24]. Let the 1kg mass be uniformly distributed over the $0.3\text{m} \times 0.2\text{m} \times 0.1\text{m}$ manipulator end effector platform and let gravity be assumed to act in the $-Z$ direction. To allow for visualisation of the workspace, in this example the constant orientation with no rotation will be utilised.

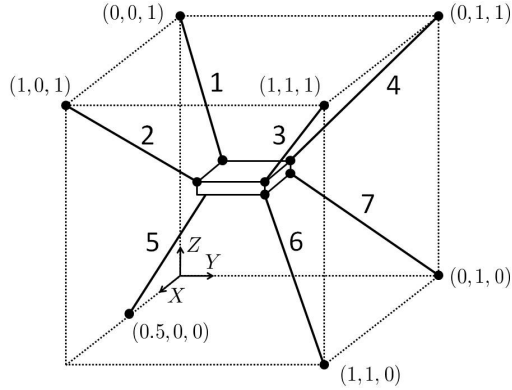


Figure 12: 6DOF Spatial Cable Driven Manipulator

Figures 13 and 14 show the x - y cross sections of the SEACM and WCW at different values of z . For this mechanism, the SEACM was computed with $0 \leq f_i \leq 1000\text{N}$ for all $i \in \{1, \dots, 7\}$ and a uniform sampling of 0.01m was used. In a similar manner to Section 5.2, it can be observed that the SW possesses greater workspace volume compared to the WCW. Utilising the information obtained from the MCS and ACM, the favourable regions of operation for this mechanism can also be observed where it is noted that both the MCS and SEACM are predominately larger towards the middle of the workspace.

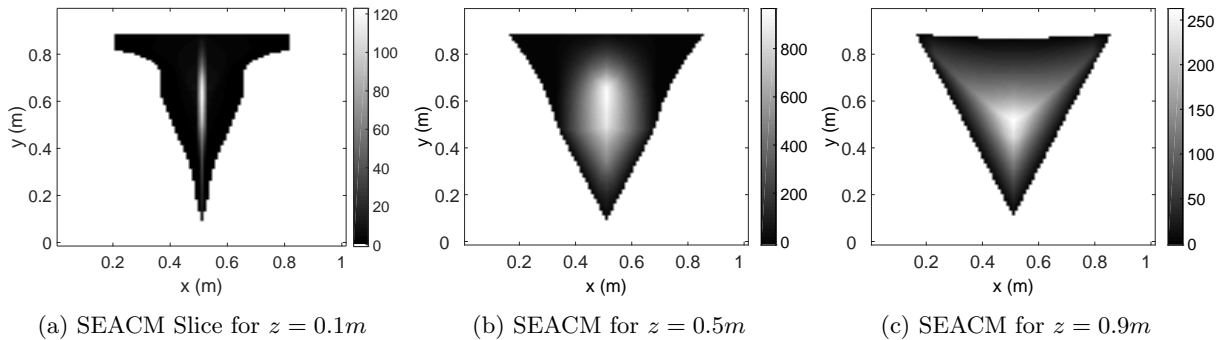


Figure 13: SEACM Slices for the Spatial Manipulator

Figure 15 depicts the MCS measure over a set of constant orientation slices at different values of z . It can be observed from Figures 13 and 15 that the mechanism is again more capable of generating motion at poses that lie within a subset of the WCW. Using these measures, the speed at which the task should be carried out can be estimated in a manner which considers the cable force limits.

5.4. Further Discussion

The available acceleration set and positive controllability theory can be used as a means of understanding motion generation capability. Compared to the restriction of the mechanism's operation to the WCW, the

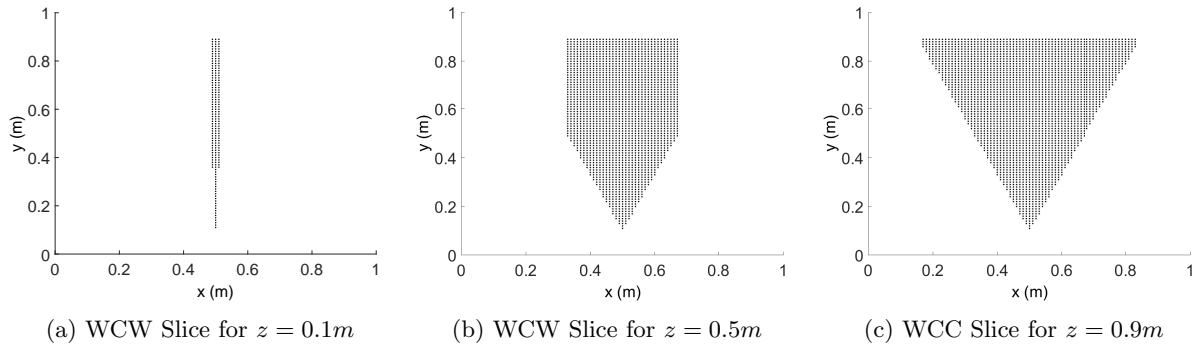


Figure 14: WCW Slices for the Spatial Manipulator

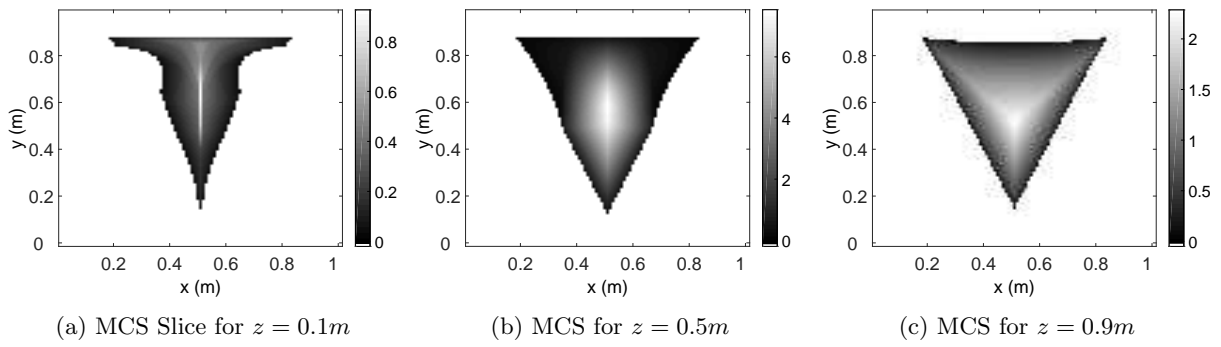


Figure 15: MCS Slices for the Spatial Manipulator

proposed method identifies a larger number of poses as being feasible for producing motion. The evaluation of the proposed metrics also provides new insight into the motion generation capability of CDRs throughout their entire workspaces. In contrast to trajectory planning methods such as [5, 9, 10, 11], this new insight provides additional understanding of the capability within the SW. Particularly it is shown that the SW can be used not only for task scaling, where the path must be known in advance, but also for path planning, where the proposed metrics can be used to facilitate online operation of motion generation algorithms through the construction of kinematic limits.

It should be noted that the proposed approach can require high resolution sampling of the joint space in addition to the filtering of information over potentially large regions. Maintaining the same resolution for higher dimensional CDR analysis will result in an exponential growth in both the computational time and memory. Such computational burden is an artefact of the use of workspace analysis and cannot be avoided. However, the effect of this growth can be mitigated by using a multi layered discretisation of the workspace and/or restrictions of the analysis to certain subsets of the operating range. In the case of the filtering method used in Section 4, it was observed that the filtering results in an increase in computational time but not in memory. In designing a workspace for analysing motion generation capability, the maximum controllable speed only needs to be computed once and can be subsequently used in the motion planning and control in order to reduce the computation required for real-time implementation.

6. Conclusion

The available acceleration set was presented and used to derive two new metrics for the study of motion generation capability of CDRs: the *static equilibrium acceleration capability measure (SEACM)* and the *maximum controllable speed (MCS)*. Using the available acceleration set, the acceleration capability measure was defined to represent the maximum acceleration that could be produced from a given set of desired kinematics. From this, it was proven that the static workspace with positive acceleration capability is locally positive controllable and can be used within the study of motion generation. Using the acceleration capability measure and positive controllability theory, the maximum controllable speed metric was also computed as an estimate of the maximum speed in which the CDR could maintain positive controllability. The insight provided by the measures was demonstrated on two different types of CDR. Future work will focus on deriving even less conservative estimates of the maximum controllable speed and on applying the acceleration set to other problems such as forward dynamics and CDR design synthesis.

7. References

- [1] J. Albus, R. Bostelman, and N. Dagalakis, "The NIST robocrane," *Journal of Robotic Systems*, vol. 10, no. 5, pp. 709–724, 1993.
- [2] L. Cone, "Skycam - an aerial robotic camera system," *Byte*, vol. 10, no. 10, p. 122, 1985.
- [3] Y. Mao, X. Jin, and S. K. Agrawal, "Real-time estimation of glenohumeral joint rotation center with cable-driven arm exoskeleton (carex) a cable-based arm exoskeleton," *Journal of Mechanisms and Robotics*, vol. 6, no. 1, p. 014502, 2014.
- [4] D. Lau, D. Oetomo, and S. K. Halgamuge, "Generalized modeling of multilink cable-driven manipulators with arbitrary routing using the cable-routing matrix," *IEEE Transactions on Robotics*, vol. 29, pp. 1102–1113, 2013.
- [5] A. Trevisani, "Planning of dynamically feasible trajectories for translational, planar, and underconstrained cable-driven robots," *Journal of Systems Science and Complexity*, vol. 26, no. 5, pp. 695–717, 2013.
- [6] A. B. Alp and S. K. Agrawal, "Cable suspended robots: design, planning and control," in *Proc. IEEE International Conference on Robotics and Automation*, vol. 4. IEEE, 2002, pp. 4275–4280.
- [7] D. Lau, D. Oetomo, and S. K. Halgamuge, "Inverse dynamics of multilink cable-driven manipulators with the consideration of joint interaction forces and moments," *IEEE Transactions on Robotics*, vol. 31, no. 2, pp. 479–488, 2015.
- [8] D. Lau, K. Bhalerao, D. Oetomo, and S. K. Halgamuge, "On the task specific evaluation and optimisation of cable-driven manipulators," in *Advances in Reconfigurable Mechanisms and Robots I*. Springer, 2012, pp. 707–716.
- [9] S. Behzadipour and A. Khajepour, "Time-optimal trajectory planning in cable-based manipulators," *IEEE Transactions on Robotics*, vol. 22, no. 3, pp. 559–563, 2006.
- [10] C. Gosselin, P. Ren, and S. Foucault, "Dynamic trajectory planning of a two-dof cable-suspended parallel robot," in *IEEE International Conference on Robotics and Automation (ICRA)*, 2012, pp. 1476–1481.
- [11] C. Gosselin and S. Foucault, "Dynamic point-to-point trajectory planning of a two-dof cable-suspended parallel robot," *IEEE Transactions on Robotics*, vol. 30, no. 3, pp. 728–736, 2014.

- [12] P. Bosscher and I. Ebert-Uphoff, “Wrench-based analysis of cable-driven robots,” in *2004. Proc. IEEE International Conference on Robotics and Automation*, vol. 5. IEEE, 2004, pp. 4950–4955.
- [13] S. Bouchard, C. Gosselin, and B. Moore, “On the ability of a cable-driven robot to generate a prescribed set of wrenches,” *Journal of Mechanisms and Robotics*, vol. 2, no. 1, p. 011010, 2010.
- [14] F. Guay, P. Cardou, A. L. Cruz-Ruiz, and S. Caro, “Measuring how well a structure supports varying external wrenches,” in *New Advances in Mechanisms, Transmissions and Applications*. Springer, 2014, pp. 385–392.
- [15] J. K. Salisbury and J. J. Craig, “Articulated hands force control and kinematic issues,” *The International Journal of Robotics Research*, vol. 1, no. 1, pp. 4–17, 1982.
- [16] R. Kurtz and V. Hayward, “Dexterity measures with unilateral actuation constraints: the $n+1$ case,” *Advanced Robotics*, vol. 9, no. 5, pp. 561–577, 1994.
- [17] C. B. Pham, S. H. Yeo, G. Yang, I. Chen *et al.*, “Workspace analysis of fully restrained cable-driven manipulators,” *Robotics and Autonomous Systems*, vol. 57, no. 9, pp. 901–912, 2009.
- [18] A. L. C. Ruiz, S. Caro, P. Cardou, and F. Guay, “Arachnis: Analysis of robots actuated by cables with handy and neat interface software,” in *Cable-Driven Parallel Robots*. Springer, 2015, pp. 293–305.
- [19] P. Chiacchio, “A new dynamic manipulability ellipsoid for redundant manipulators,” *Robotica*, vol. 18, no. 04, pp. 381–387, 2000.
- [20] D. Lau, J. Eden, D. Oetomo, and S. K. Halgamuge, “Musculoskeletal static workspace analysis of the human shoulder as a cable-driven robot,” *IEEE/ASME Transactions of Mechatronics*, vol. 20, no. 2, pp. 978–984, 2014.
- [21] G. Barrette and C. M. Gosselin, “Determination of the dynamic workspace of cable-driven planar parallel mechanisms,” *Journal of Mechanical Design*, vol. 127, no. 2, pp. 242–248, 2005.
- [22] M. Gouttefarde, D. Daney, and J.-P. Merlet, “Interval-analysis-based determination of the wrench-feasible workspace of parallel cable-driven robots,” *IEEE Transactions on Robotics*, vol. 27, no. 1, pp. 1–13, 2011.
- [23] M. Gouttefarde and C. M. Gosselin, “Analysis of the wrench-closure workspace of planar parallel cable-driven mechanisms,” *IEEE Transactions on Robotics*, vol. 22, no. 3, pp. 434–445, 2006.
- [24] D. Lau, D. Oetomo, and S. K. Halgamuge, “Wrench-closure workspace generation for cable driven parallel manipulators using a hybrid analytical-numerical approach,” *Journal of Mechanical Design*, vol. 133, no. 7, p. 071004, 2011.
- [25] S. Lahouar, E. Ottaviano, S. Zeghoul, L. Romdhane, and M. Ceccarelli, “Collision free path-planning for cable-driven parallel robots,” *Robotics and Autonomous Systems*, vol. 57, no. 11, pp. 1083–1093, 2009.
- [26] I. Ebert-Uphoff and P. A. Voglewede, “On the connections between cable-driven robots, parallel manipulators and grasping,” in *Proc. IEEE International Conference on Robotics and Automation*, vol. 5. IEEE, 2004, pp. 4521–4526.
- [27] N. Zhang and W. Shang, “Dynamic trajectory planning of a 3-dof under-constrained cable-driven parallel robot,” *Mechanism and Machine Theory*, vol. 98, pp. 21–35, 2016.
- [28] H. Yoshida and T. Tanaka, “Positive controllability test for continuous-time linear systems,” *IEEE Transactions on Automatic Control*, vol. 52, no. 9, pp. 1685–1689, 2007.
- [29] R. F. Brammer, “Controllability in linear autonomous systems with positive controllers,” *SIAM Journal on Control*, vol. 10, no. 2, pp. 339–353, 1972.
- [30] J. Eden, Y. Tan, D. Lau, and D. Oetomo, “On the positive output controllability of linear time invariant systems,” *Automatica*, vol. 71, pp. 202–209, 2016.
- [31] D. Lau, J. Eden, Y. Tan, and D. Oetomo, “CASPR: A comprehensive cable-robot analysis and simulation platform for the research of cable-driven parallel robots,” in *IEEE/RSJ International Conference on Intelligent Robots and Systems (IROS)*. IEEE, 2016.
- [32] A. T. Riechel and I. Ebert-Uphoff, “Force-feasible workspace analysis for underconstrained, point-mass cable robots,” in *Proceedings IEEE International Conference on Robotics and Automation*, vol. 5, 2004, pp. 4956–4962.
- [33] M. Gouttefarde, J.-F. Collard, N. Riehl, and C. Baradat, “Geometry selection of a redundantly actuated cable-suspended parallel robot,” *IEEE Transactions on Robotics*, vol. 31, no. 2, pp. 501–510, 2015.
- [34] D. Lau, J. Eden, S. K. Halgamuge, and D. Oetomo, “Cable function analysis for the musculoskeletal static workspace of a human shoulder,” in *Cable-Driven Parallel Robots*. Springer, 2015, pp. 263–274.
- [35] J. I. Mulero-Martínez, “Uniform bounds of the coriolis/centripetal matrix of serial robot manipulators,” *IEEE Transactions on Robotics*, vol. 23, no. 5, pp. 1083–1089, 2007.
- [36] S. M. LaValle, *Planning algorithms*. Cambridge university press, 2006.
- [37] S. Sastry, *Nonlinear systems: analysis, stability, and control*. Springer New York, 1999, vol. 10.

Appendix A. Proof of Theorem 1

Proof. By definition, for any locally positive controllable state \mathbf{x}^* , there exists a finite time T , an input sequence $\mathbf{u}(t) \geq 0, \forall t \in [0, T]$ and a positive number $\epsilon > 0$ such that at time T the system can reach any neighbouring state $\mathbf{x} \in \mathcal{B}(\mathbf{x}^*, \epsilon)$. Since the set is connected, a connected path between any two states can always be defined by using a finite sequence of paths connecting neighbour states. An input sequence to connect any two states within the region in finite time is therefore given by concatenating the input sequences that connect each of the neighbouring states. \square

Appendix B. Proof of Theorem 2

Controllability is a property that is invariant to control input [37]. The state $\mathbf{x} = [\mathbf{q}^{*T} \ \mathbf{0}^T]^T$ of the CDR with dynamics (1) is therefore locally positive controllable if it can be shown that the system is locally feedback equivalent to a known locally controllable system using only non-negative control input.

Let

$$\mathbf{z} = \begin{bmatrix} (\mathbf{q} - \mathbf{q}^*) \\ \dot{\mathbf{q}} \end{bmatrix}. \quad (\text{B.1})$$

Since $\varrho(\mathbf{q}^*) > 0$, then there exists a neighbourhood about $[(\mathbf{q}^*)^T \ \mathbf{0}^T]^T$, a positive number e and a virtual control input $\mathbf{v} \in \mathbb{R}^d$ in which a cable force $\mathbf{f}^* \geq \mathbf{0}$ can be chosen such that

$$-\mathcal{L}(\mathbf{q})^T \mathbf{f}^* = -M^{-1}(\mathbf{q}) (\mathbf{C}(\mathbf{q}, \dot{\mathbf{q}}) + \mathbf{G}(\mathbf{q}) + \mathbf{v}), \quad (\text{B.2})$$

where $\|\mathbf{v}\| \leq e$. Applying the force \mathbf{f}^* , it can be seen that (1) is locally feedback equivalent to the fully actuated system

$$\dot{\mathbf{z}} = \begin{bmatrix} 0 & I \\ 0 & 0 \end{bmatrix} \mathbf{z} + \begin{bmatrix} 0 \\ I \end{bmatrix} \mathbf{v}, \quad \|\mathbf{v}\| \leq e. \quad (\text{B.3})$$

This system is a double integrator which is locally controllable for the given actuation limits. As a result the system described by (1) is locally positive controllable at \mathbf{q}^* . \square